Inorganica Chimica Acta 597 (2026) 123180

Contents lists available at ScienceDirect

Inorganica Chimica Acta

journal homepage: www.elsevier.com/locate/ica

Investigations into cerium(III) and cerium(IV) nitrate complexes with tris-1-naphthylyphosphine oxide and bis-1-naphthlyalklyphosphine oxides

Simon J. Coles [a], Simon Cooper [b], Wim T. Klooster [a], Laura J.McCormick McPherson [a], Andrew W.G.Platt [b,*]

[a] UK National Crystallography Service, Chemistry, University of Southampton, Highfield Campus, Southampton SO17 1BJ, UK
[b] School of Justice, Security and Sustainability, University of Staffordshire, Science Centre, Leek Road, Stoke on Trent ST4 2DF, UK

ARTICLE INFO

Keywords:
Cerium
Phosphine oxide
NMR, crystal structures
Mass spectrometry

ABSTRACT

The reaction between ammonium cerium(IV) nitrate (CAN) and tris-1-naphthylphosphine oxide (Nap_3PO, L^1), bis-1-naphthylmethlyphosphine oxide (Nap_2MePO, L^2) and bis-1-naphthylethlyphosphine oxide (Nap_2EtPO, L^3) have been investigated. The ^{31}P NMR spectra show that complex formation occurs readily in CD_3CN solution and more slowly in $CDCl_3$. Isolation of bulk Ce(IV) complexes was difficult due to decomposition to Ce(III) during crystallisation. The Ce(IV) complexes can be characterised in solution by multinuclear NMR (^1H, ^{13}C and ^{31}P) spectroscopy and show that decomposition to Ce(III) occurs in CD_3CN with Ce(IV) being more stable in $CDCl_3$. The structures of the ligands Nap_2MePO and Nap_2EtPO and the complexes $[Ce(NO_3)_3(Nap_2MePO)_3]$, $[Ce(NO_3)_3(Nap_2EtPO)_3]$ and $[Ce(NO_3)_4(Nap_2EtPO)_2]$ have been determined. Ce(IV) solutions undergo reduction to Ce(III) during the electrospray ionisation mass spectra process. The tandem mass spectra of $[Ce(NO_3)_2L_n]^+$ show that loss of ligand is favoured for for high values of n whilst for $n = 2$ loss of NO_2 generating Ce(IV) oxo complexes is increasingly important.

1. Introduction

Cerium(IV) is the most stable +4 oxidation state in lanthanide series due to its $4f^0$ electronic configuration and it thus has the most extensive coordination chemistry amongst their tetravalent ions[1]. There is considerable interest in applications of Ce(IV) coordination complexes. Catalytic photooxidation, decarboxylation and oxygenation of arylacetic acids by $Ce(OR)_4$ and $Ce(O_2CR)_4$ occurs due to Ce(III) / Ce(IV) cycling under an atmosphere of oxygen [2]. The carbonate complex $[CpCo(PO(OEt)_2)_3]CeCO_3$ acts as a catalytic precursor for similar reactions under visible light irradiation [3]. The cerium mediated formation of bibenzofuranones is also promoted by visible light [4]. A stochiometric reaction mediated by Ce(IV) allows the mild ring opening of hydroxycyclobutanes to produce γ-fluoroketones [5], whilst a cerium (IV) intermediate has been identified during photocatalytic activation of C—I bonds by $[CeCl_6]^{3-}$[6]. Metal organic frameworks containing Ce (IV) have also been used as heterogeneous and homogeneous catalysts for a variety of reactions [7] and to promote the CO_2 fixation with styrenes to give styrene carbonates [8]. Cerium(IV) complexes are the reactive intermediates in the photocatalytic [9] and electrocatalytic activation [10] of alkanes, and have biological activity, with a pyridine dicarboxylate complex active against a human colon adenocarcinoma cell line [11]. Some of these applications are summarised in Scheme 1.

Cerium(IV) forms particularly stable complexes, mainly with O and N donors [12]. Within the O-donors phosphine oxides are relatively under reported [12,13], and since the initial reports of $[Ce(NO_3)_4(Ph_3PO)_2]$ [14,15] only a few have been structurally characterised. The tricyclohexylphosphine oxide complex, $[Ce(NO_3)_4(Cy_3PO)_2]$ adopts a bicapped square antiprismatic geometry and is structurally similar to Ph_3PO analogue and the cationic $[Ce(NO_3)_3(Et_3PO)_3]^+$ is a tricapped trigonal prism[16]. With the bidentate 4,5-bis(diphenylphosphine oxide)-9,9-dimethylxanthene, and 1,2-bis (diphenylphosphino)ethane dioxides 10-coordinate cationic complexes of the form $[Ce(NO_3)_3L_2]^+$ are formed [17]. In view of the wide and diverse variety of applications of Ce(IV) complexes and the relative lack of structural data in this area, we felt a further investigation of Ce(IV) phosphine oxide complexes was warranted. We chose to explore the complexes of ligands with naphthyl substituents as, due to their extended π-systems, they have the potential to act as photosensitisers which could lead to application as photocatalysts. The effect of the

* Corresponding author.
E-mail address: a.platt@staffs.ac.uk (A. W.G.Platt).

https://doi.org/10.1016/j.ica.2026.123180
Received 29 January 2026; Received in revised form 19 March 2026; Accepted 22 March 2026
Available online 23 March 2026

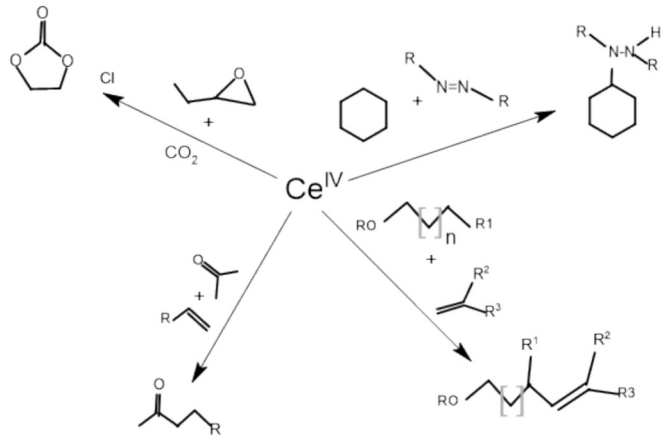

Scheme 1. Some applications of Ce(IV) complexes in organic transformations.

increased steric bulk on the geometry and properties of their Ce(IV) complexes has not been studied before and is thus of interest from a structural chemistry point of view.

2. Results and discussion

Nap_3PO, L^1, was prepared by oxidation of the phosphine with H_2O_2 in acetone as described previously [19] and Nap_2RPO (R = Me L^2, R = Et L^3) by quaternisation of Nap_3P with RI in acetonitrile followed by hydrolysis of the isolated phosphonium salt with ethanolic KOH.

2.1. Solution studies

NMR spectroscopy is a very powerful tool for the study of reactions in solution. In this instance we anticipated that ^{31}P NMR would be an effective technique due to its excellent ability to distinguish between diamagnetic and paramagnetic complexes of cerium on the basis of chemical shift alone.

The reactions between ceric ammonium nitrate (CAN) and L^1, L^2 and L^3 were studied in a variety of solvents. In $CDCl_3$ there was no reaction between L^1 and a suspension of CAN, with or without ultrasonic agitation. The only ^{31}P NMR signal observed was that of the free ligand at 41.8 ppm. Similarly, in CD_3NO_2 and acetone-d_6 no reaction was observed possibly due to the very low solubility of L^1 in these solvents. In CD_3CN with a 1:2 ratio of CAN:L^1 a number of complexes appear to be initially formed with resonances observed at 54.9, 53.8 and 50.1 ppm. The chemical shifts are in the range of similar Ce(IV) complexes [17] and are clearly very different from the shift of the free ligand and to those of Ce(III) complexes which show significant paramagnetic effects with chemical shifts in the region of 70–80 ppm. On standing, the spectrum simplified and a single peak at 51.6 ppm was seen and tentatively assigned as $[Ce(NO_3)_4L^1_2]$. All species have low solubility, and lengthy accumulations of the order of 30,000 scans were required to obtain satisfactory spectra. We were unable to obtain solid crystalline materials from these solutions which would have allowed further

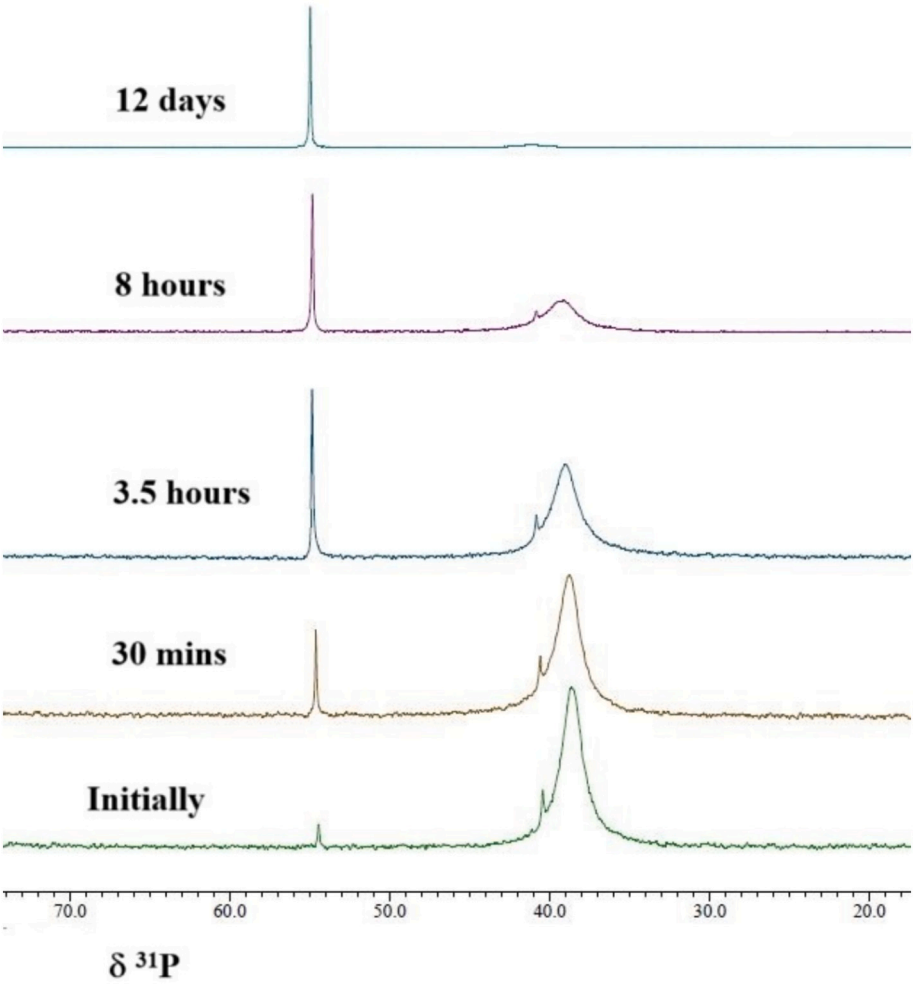

Fig. 1. The ^{31}P NMR spectra of the reaction of L^3 with CAN in $CDCl_3$.

characterisation. This behaviour is similar in this respect to that of the reactions of L^1 with lanthanide nitrates where complexes with lighter metals could not be isolated [18].

The reactions of an excess of solid CAN with both L^2 and L^3 in $CDCl_3$ showed the slow reduction in intensity of the signal from the free ligand at about 34 ppm and a corresponding increase in intensity of peaks at around 53.5 and 55.0 ppm assigned as $[Ce(NO_3)_4L^2_2]$ and $[Ce(NO_3)_4L^3_2]$ respectively. Very low intensity signals at about 41 ppm were seen in both reactions and are tentatively assigned to a 1:1 complex. The spectra for the reaction of L^3 with CAN are shown in Fig. 1.

On standing for 12 d at 30 °C in $CDCl_3$ solution there was no indication of decomposition to cerium(III).

The solubility of L^2 and L^3 in CD_3CN is low. The ^{31}P NMR spectra with high ratios of L^2:Ce show the formation of two cerium(IV) complexes (δ = 46.0 and 54.8 ppm) in addition to the signal from unreacted free ligand. In the presence of an excess of CAN only the signal at 54.8 ppm, tentatively assigned to $[Ce(NO_3)_4L^2_2]$, was observed. On standing for 7 days decomposition to Ce(III) was apparent with broad peak at 74.3 ppm ($w_{1/2}$ = 245 Hz) present in addition to that of unreduced complex. Reactions with L^3 follow a similar pattern. With a 2:1 ratio of L: CAN the ^{31}P NMR spectrum showed single resonance at 56.2 ppm assigned as $[Ce(NO_3)_4L^3_2]$. On standing over 2 weeks substantial decomposition was apparent with a signal at 76.7 ppm Ce(III) present in an approximately 1:1 ratio of Ce(III):Ce(IV) and a low intensity resonance at 45.0 ppm similar to that observed in the L^2 reaction.

As the Ce(IV) complexes are relatively stable in $CDCl_3$ they were studied by multinuclear (^1H, ^{13}C and ^{31}P) NMR spectroscopy. We were particularly interested in studying the coordination shifts as these can give an indication of electron density changes on binding to Ce(IV).

Assignments in the ^1H spectra of the free ligands were based on the highest frequency signal being H_8 [19]. This assignment and that of the H_2 signal were confirmed by the observation of cross peaks with the methyl and methylene signals in the NOESY spectra of the L^2 and L^3 complexes respectively. Assignments of the remaining ^1H signals were made by COSY to identify adjacent protons, some of which were also confirmed by the observation of cross peaks in the NOESY spectrum. The ^{13}C signals were assigned by use of HMQC heteronuclear ^1H—^{13}C correlation spectra. The assignments of the C_{4a} and C_{8a} signals were made by using long range correlations (HMBC) to H_8 and H_5. The assignments for the free ligands and their complexes are given in Table S1 - S3. The coordination shifts for the ^1H, ^{13}C and ^{31}P NMR spectra are shown in Table 1.

The effects are shown schematically in Fig. 2. As expected, the ^{31}P spectra show strong deshielding on coordination to the Ce ions, with C_6 and H_6 also being strongly deshielded.

In general, the nuclei are more shielded on coordination to the highly charged cerium ion. This pattern of coordination shifts differs from that previously observed in the ^1H and ^{13}C NMR for aromatic pyridine or Shiff base systems [20,21] where the coordinating atoms form part of the aromatic system. Here the naphthyl rings are removed from the coordination site and there is no overall deshielding effect. There are no strong correlations of Δ_{coord} with either the number of bonds through which inductive effects could be transmitted, or the distance between the target nucleus and the Ce(IV) centre.

2.2. Structural studies

Attempted crystallisations from the NMR solutions containing initially only Ce(IV) was made by slow evaporation of the solutions. This procedure generally yielded Ce(III) complexes of L^2 (from $CDCl_3$) and L^3 (from CD_3CN). In one instance, however, a Ce(IV) complex of L^3 was obtained by slow evaporation of a $CDCl_3$ solution and its structure, together with those of the Ce(III) complexes isolated in a similar manner are discussed below.

Details of the data collection and refinement of the ligands and their complexes are given in Table S4 in the supplementary information. The structure of Nap_3PO has been reported previously [19] and those of L^2 and L^3 were determined for comparison with their complexes. The structure of L^2 is shown in Fig. 3 and selected bond distances and angles for both the ligands and their complexes are given in Table 2. A full list of bond distances and angles can be found in the supplementary information.

The ligands crystallise in orthorhombic and monoclinic space groups for the methyl and ethyl derivatives, respectively. The P═O and P—C distances and angles around the P-atom in L^1 and L^2 are essentially the same and do not differ significantly from those found in Nap_3PO[19].

There are short intra and intermolecular contacts between the phosphoryl oxygen atoms and hydrogen atoms on the naphthyl rings. The average values of these are indicated in Fig. 4 for both the free ligands and their Ce(III) and Ce(IV) complexes.

Table 1
^1H, ^{13}C and ^{31}P chemicals shifts and coordination shifts Δ_{coord}, ($\delta_{complex} - \delta_{ligand}$) /ppm in Ce(IV) complexes in $CDCl_3$.

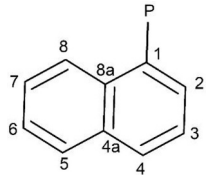

	L^2		$Ce(NO_3)_4L^2_2$				L^3		$Ce(NO_3)_4L^3_2$			
	^1H	^{13}C	^1H	ΔH_{coord}	^{13}C	ΔC_{coord}	^1H	^{13}C	^1H	ΔH_{coord}	^{13}C	ΔC_{coord}
CH_3	2.31	18.3	2.53	0.22	15.8	−2.5	1.18	6.3	1.00	−0.18	5.8	−0.5
CH_2							2.62	23.6	2.93	0.31	21.5	−2.1
1		130.7			125.0	−5.7		129.5			123.9	−5.6
2	7.88	129.1	7.93	0.05	124.9	−4.2	7.92	132.3	7.81	−0.11	124.7	−7.6
3	7.50	124.7	7.33	−0.17	128.1	3.4	7.51	124.4	7.38	−0.13	126.8	2.4
4	8.01	133.1	7.43	−0.58	127.0	−6.1	8.01	134	7.22	−0.79	128.1	−5.9
4a		133.9			132.1	−1.8		133.4			132.1	−1.3
5	7.91	131.6	7.84	−0.07	129.4	−2.2	7.86	129	7.81	−0.05	129.3	0.3
6	7.45	126.5	8.07	0.62	135.3	8.8	7.47	126.4	8.07	0.60	135	8.6
7	7.42	127.4	7.59	0.17	125.2	−2.2	7.4	127.3	7.62	0.22	125.1	−2.2
8	8.61	126.6	8.16	−0.45	132.8	6.2	8.57	126.7	8.22	−0.35	133.3	6.6
8a		133.3			133.8	0.5		133.5			133.7	0.2
	^{31}P					ΔP_{coord}					ΔP_{coord}	
^{31}P	34.2		51.2			17.0	39.2		54.9		15.7	

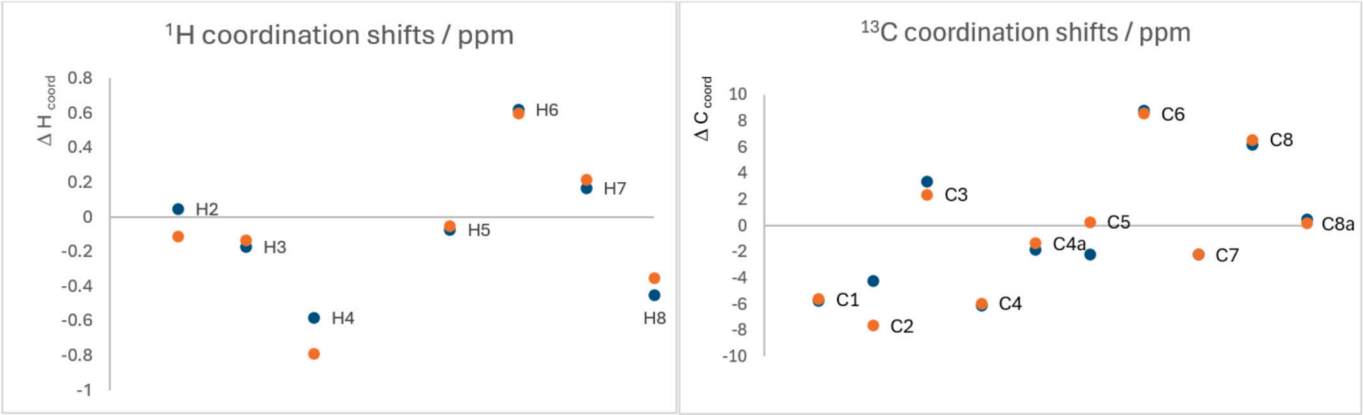

Fig. 2. A schematic representation of the coordination shifts in the ^{1}H, ^{13}C spectra of L^2 (blue circles) and L^3 (orange circles) on coordination to Ce(IV).

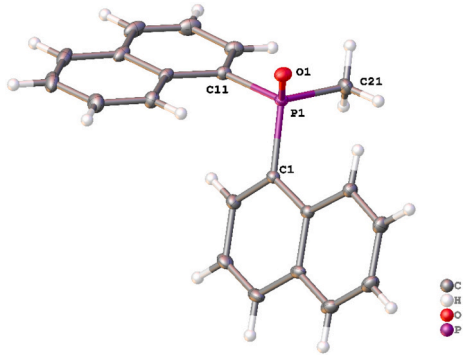

Fig. 3. The structure of L^2. Thermal ellipsoids drawn at the 50% probability level.

The Ce(III) complexes can be visualised as pseudo-octahedral if the nitrates are thought of as monodentate ligands bonded via the N-atom. In this formalism both complexes adopt the pseudo-meridonal arrangement which is common in lanthanide nitrate complexes with phosphine oxides of low to moderate steric requirements [13]. Here the substitution of one of the naphthyl rings for a sterically less demanding alky group reduces the overall crowding in the complex compared to Nap_3PO complexes where only two phosphine oxides are directly bonded to the metal [18]. The detailed geometries of the complexes were determined by Shape analysis [22,23] where standard geometries for a given coordination polyhedron are compared with the observed structure. The goodness of fit is given by the S-parameter where $0.1 < S < 3$ represent small distortions from the idealised geometry. Both $[Ce(NO_3)_3L^2_3]$ and $[Ce(NO_3)_3L^3_3]$ are best described as 1:5:3 muffins, S = 2.278 and 3.956 for the methyl and ethyl derivatives respectively. The apex is O1 (PO) and the 5 set comprises O2(PO), O101, O104, O107 and O108 and the 3 set consists of O3(PO), O102 and O105. The structure of $[Ce(NO_3)_3L^2_3]$ is shown in Fig. 5 together with a representation of the 1:5:3 coordination geometry.

The structure of the Ce(IV) complex is a distorted 2:4:2:2 sphenocorona and the structure together with a representation of the coordination geometry is given in Fig. 6. The distortion from the idealised geometry (S = 3.52) is relatively small with the next best fit being to a square antiprism (S = 4.13).

The Ce(III)-O distances fall within the range of values observed in other 9-coordinate Ce(III) complexes, 2.42–2.32 Å for PO-Ce and 2.64–2.46 Å for NO-Ce [24–26]. Similarly, the average Ce(IV)-O distances in $Ce(NO_3)_4(Nap_2EtPO)_2$ of 2.235 Å and 2.472 Å for (P)O-Ce and (N)O-Ce respectively lie within the range for other Ce(IV) nitrate complexes with aromatic phosphine oxides, which are 2.215–2.234 Å and 2.437–2.592 Å [14,15,17]. Thus, the presence of two bulky substituents on the P atoms does not lead to significant changes in the coordination environment around the Ce(III) or Ce(IV) ions. This contrasts with the situation for Nap_3PO complexes with lanthanide nitrates where a lengthening of the Ln-O(P) bonds compared to complexes with less bulky ligands was found [19].

As expected, the P═O distances increase on coordination for both Ce(III) and Ce(IV) with a larger change on coordination to Ce(IV) due to the higher charge on the metal. The P—C bond distances within the coordinated ligands all decrease slightly on binding to the metal, again with larger differences observed for Ce(IV) as shown in Table 2.

2.3. *Electrospray ionisation mass spectrometry*

The electrospray ionisation mass spectra for the ligands were obtained from CH_3CN solution. Assignments were based on the accurate mass and the isotope distribution pattern, both of which gave good agreement with the calculated values. The spectra of the free ligands show the expected peaks for $[L + H]^+$, $[L + Na]^+$, $[2\ L + H]^+$, $[2\ L + Na]^+$,and $[3\ L + Na]^+$. For L^1 the base peak was $[L^1 + H]^+$ whilst for the other ligands $[2\ L + Na]^+$ was the most abundant ion. The results are summarised in Table S15.

Due to the propensity of the cerium(IV) species to undergo reduction in CD_3CN their spectra were obtained by injecting a $CDCl_3$ solution

Table 2
Selected Bond lengths (Å) and angles (°) in the free ligands and their complexes.

	Nap_2MePO	$Ce(NO_3)_3L^2_3$	% change	Nap_2EtPO	$Ce(NO_3)_3L^3_3$	% change	$Ce(NO_3)_4L^3_2$	% change
P=O	1.494	1.506	0.8	1.4939	1.510	1.0	1.5241	2.0
P-C(R)	1.796	1.7924	−0.2	1.8084	1.802	−0.4	1.795	−0.7
P-C(Nap)	1.8131	1.804	−0.5	1.8124	1.806	−0.4	1.798	−0.8
Ce-O(P)		2.402			2.395		2.235	
Ce-O(N)		2.593			2.592		2.478	
O-P-C(Me/Et)	112.23	111.1	−1.0	111.45	110.4	−0.9	110.07	−1.2
O-P-C(Nap)	113.39	112.5	−0.8	112.82	110.11	−2.4	109.08	−3.3

There are no significant differences in the bond distances and angles around the phosphorus atom resulting from the different R-groups.

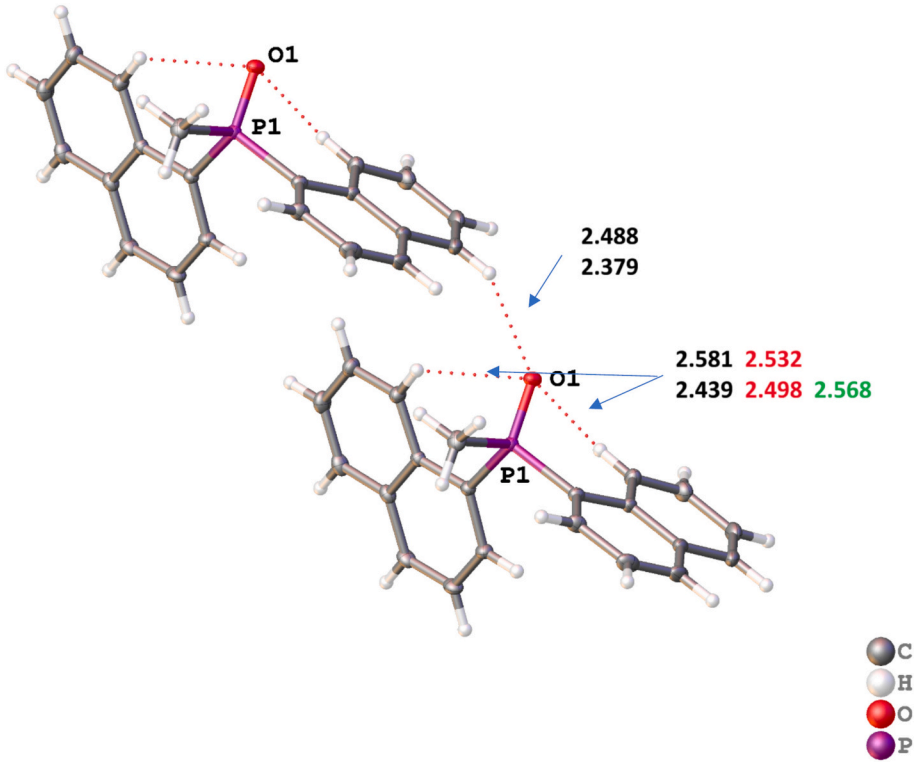

Fig. 4. The short O···H contacts (Å) in L^2 (upper number) and L^3 (lower number) and their Ce(III) (red font) and Ce(IV) (green font) complexes. (For interpretation of the references to colour in this figure legend, the reader is referred to the web version of this article.)

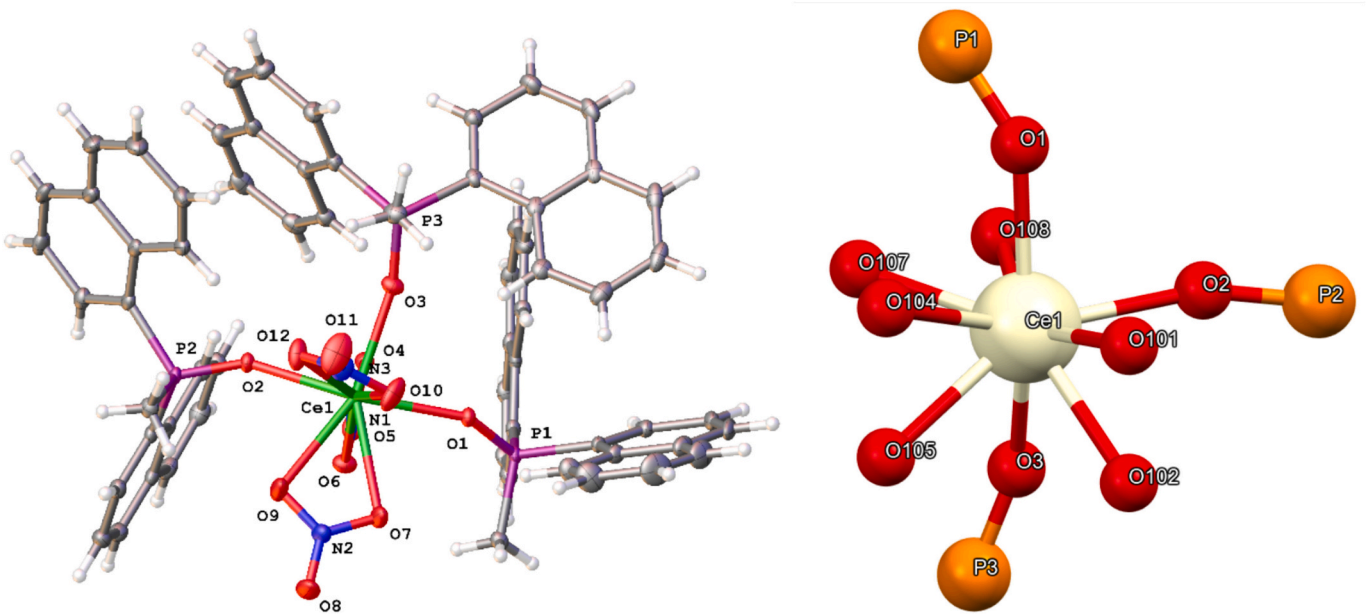

Fig. 5. The structure of $[Ce(NO_3)_3L^2_3]$ (left) Thermal ellipsoids drawn at the 50% probability level and a representation of the 1:5:3 muffin geometry (right).

known to contain only Ce(IV) by ^{31}P NMR spectroscopy, into the CH_3CN mobile phase. As it was not possible to produce the Ce(IV) complex of L^1 in $CDCl_3$ an acetonitrile solution had to be used in this instance.

In all cases the spectra are dominated by peaks due to the ligands and the only Ce(III) containing ions were observed. This is presumably because of reduction which is known to occur during ESMS for high oxidation state species [27]. It might be anticipated that parent ions derived from the reduced solid-state structure, namely $[Ce(NO_3)_2L^2_3]^+$, would be abundant in the mass spectra. Whilst this ion is intense for complexes of L^2 and L^3, ions formed by redistribution reactions such as $[Ce(NO_3)_2L^2_2]^+$ and $[Ce(NO_3)_2L^2_4]^+$ are also significant. The results are shown in Table 3 and a typical spectrum in Fig. 7.

We examined the tandem mass spectra of $[Ce(NO_3)_2L_n]^+$ ions to assess their stability in the gas phase as these might best represent species present in solution. The results are presented in Tables S15 to 17 for the ions containing L^1, L^2 and L^3 respectively and an example of the spectra obtained at varying COFF energies is shown for the $[Ce(NO_3)_2L^3_2]^+$ ion in Fig. 8.

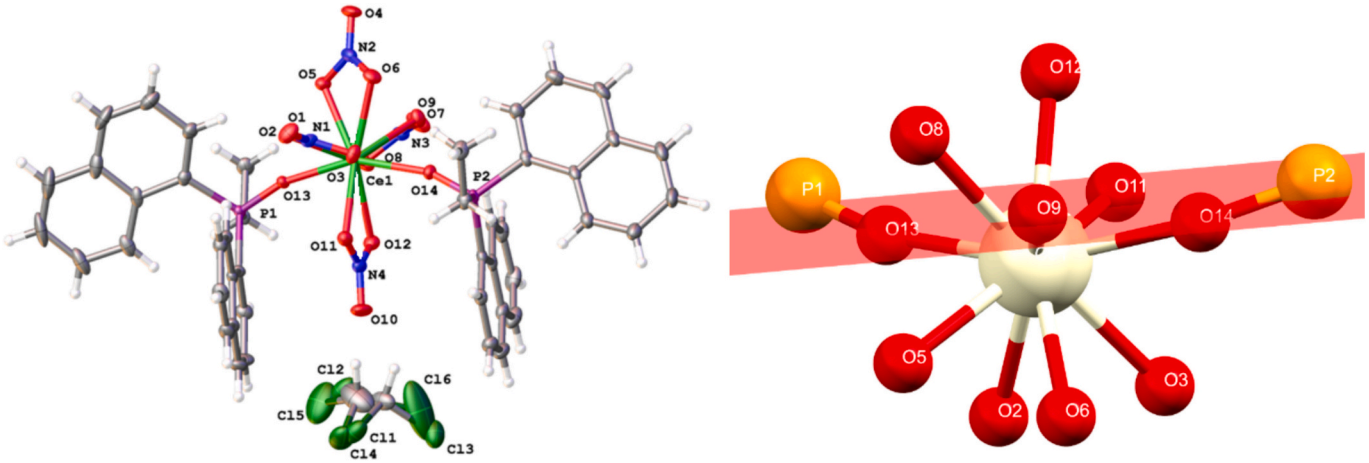

Fig. 6. The structure of $[Ce(NO_3)_4L^2_2]\cdot CDCl_3$. Thermal ellipsoids drawn at the 50% probability level and a representation of the 2:4:2:2 sphenocorona geometry (right) with the 4-plane highlighted in red. (For interpretation of the references to colour in this figure legend, the reader is referred to the web version of this article.)

Table 3
The cerium containing ions observed in the Electrospray Ionisation Mass Spectra of solutions of Ce(IV). Observed mass (abundance / %) and theoretical mass beneath in blue font (difference from calculated values /ppm).

	$L^{1\,a}$	$L^{2\,b}$	$L^{3\,b}$
$[Ce(NO_3)_2L]^+$	692.0134(2)		
	692.0141 (1)		
$[Ce(NO_3)_2L_2]^+$	1120.1467(1)	896.0848(5)	924.1165(5)
	1120.1471 (0.4)	896.0845 (0.3)	924.1158 (0.1)
$[Ce(NO_3)_2L_3]^+$	1548.2802(1)	1212.1892(20)	1254.2378(55)
	1548.2801 (0.01)	1212.1862 (2.5)	1254.2331 (3.7)
$[Ce(NO_3)_2L_4]^+$		1528.2941(40)	1584.3523(20)
		1528.2879 (4.1)	1584.3505 (1.1)

a From a CD_3CN solution containing Ce(IV) only. b. From $CDCl_3$ solutions of Ce (IV)

The major fragmentation pathway for $[Ce(NO_3)_2L_4]^+$ and $[Ce(NO_3)_2L_3]^+$ is loss of ligand which occurs at lower collision energies than for $[Ce(NO_3)_2L_2]^+$. The loss of NO_2 via an internal redox process to form Ce(IV) species such as $[CeO(NO_3)L_n]^+$ (which are not observed in the normal electrospray ionisation spectra), becomes progressively more important as n decreases, and is the main fragmentation path for $[Ce(NO_3)_2L_2]^+$ reflecting the stability of the $[CeL_2]^+$ core to further loss of ligand. Further loss of NO_2 is seen from $[CeO(NO_3)L]^+$ producing $[CeO_2L]^+$ at high collision energy. The naked $[CeO_2]^+$ radical cation has been previously observed in the gas phase by oxidation of Ce^+ by O_2 followed by NO_2 [28] and other gaseous high valent lanthanide oxo ions are well known [29–31]. This appears to be the first time that coordination complexes of $[CeO(NO_3)]^+$ and $[CeO_2]^+$ have been observed. The results for the $[Ce(NO_3)_2L^2_n]^+$ ions are summarised in Scheme 2 and are typical of the other complexes.

3. Conclusion

The formation of Ce(IV) complexes with bulky phosphine oxide ligands Nap_3PO, Nap_2MePO and Nap_2EtPO can be achieved in solution relatively easily isolation of the complexes in bulk was not achieved, with reduction to Ce(III) dominating the crystallisation processes and only one Ce(IV) complex could be isolated and that in low quantity. This precluded further work to investigate and applications. The crystal structures show that the Ce(III) forms complexes with the expected geometries, whilst the Ce(IV) complex $[Ce(NO_3)_4L^3_2]$ has a similar structure to other neutral Ce(IV) phosphine oxide complexes. The facile reduction to Ce(III) seen in attempts to grow Ce(IV) containing crystals is mirrored in the electrospray ionisation mass spectra where Ce(III) complexes are exclusively formed. The tandem mass spectra show that at high collision energy oxidation of Ce(III) by coordinated nitrate giving Ce(IV) oxo-complexes occurs. Overall the work provides an insight

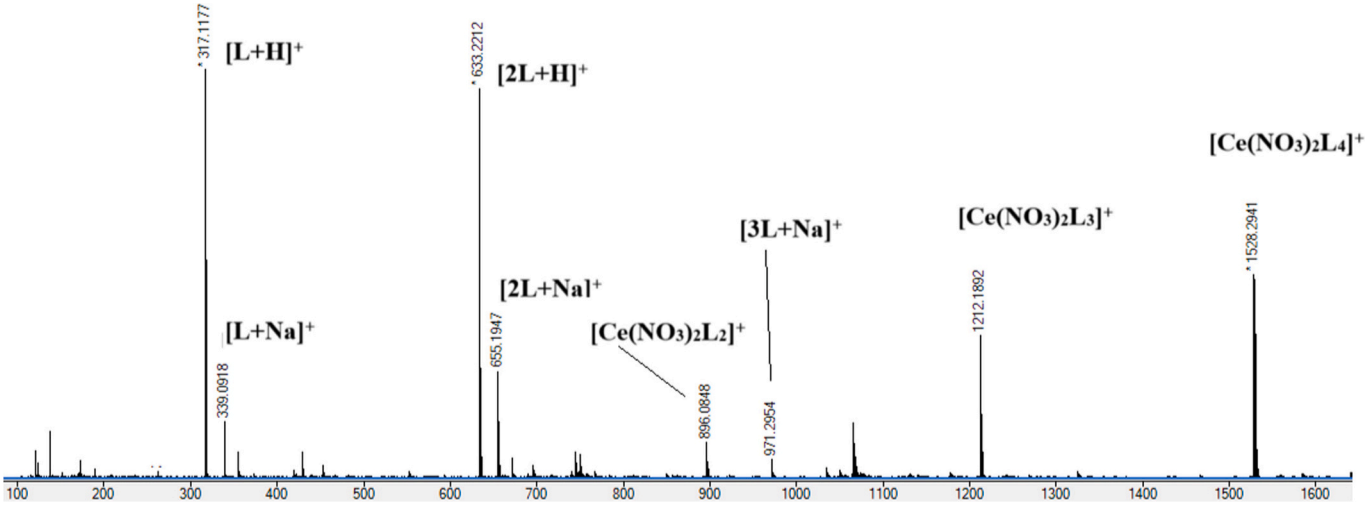

Fig. 7. The positive ion ESMS spectrum from $Ce(NO_3)_4L^2_2$ in $CDCl_3$ solution injected into a CH_3CN mobile phase.

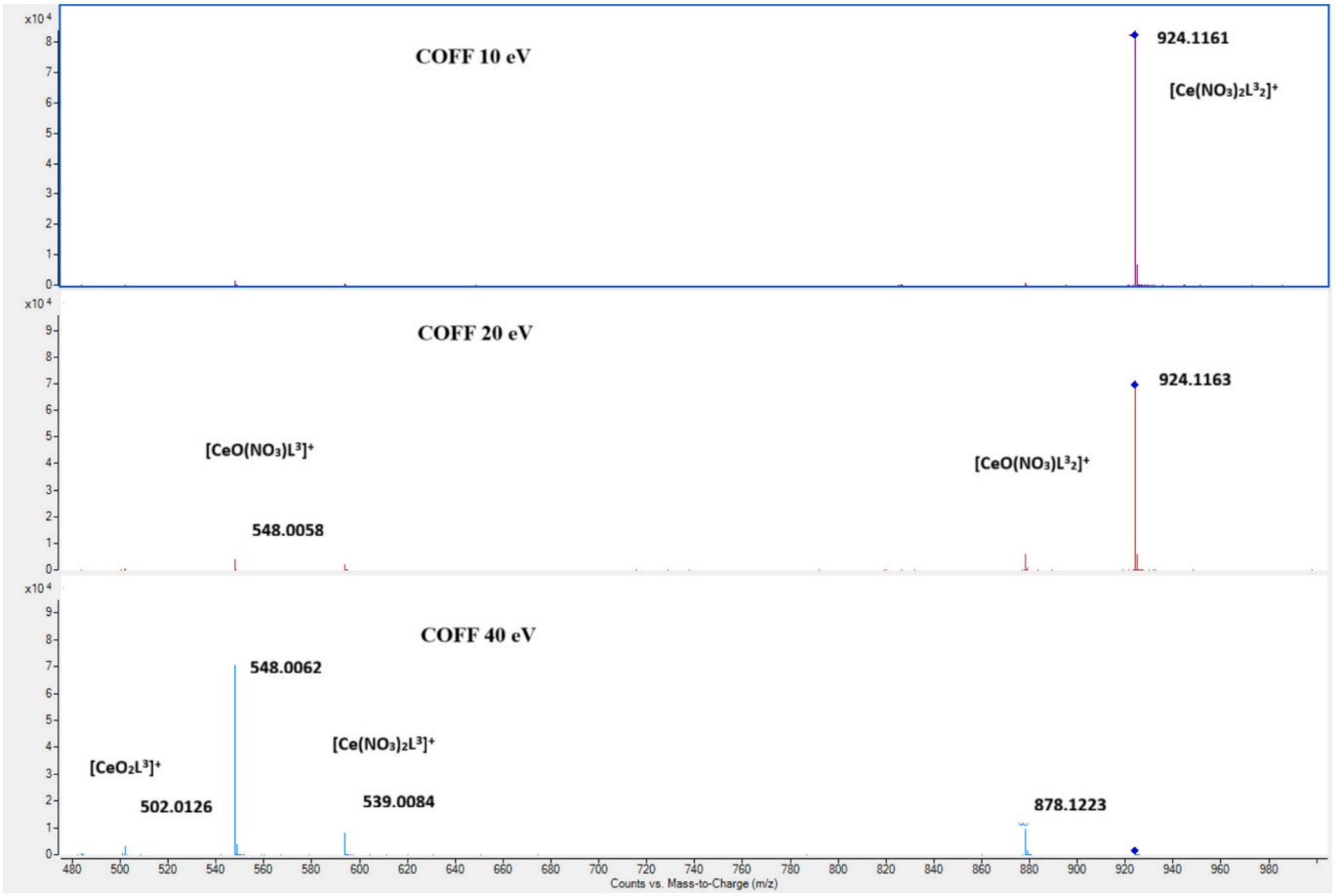

Fig. 8. The tandem mass spectra of $[Ce(NO_3)_2L^3_2]^+$ at varying collision offset voltages.

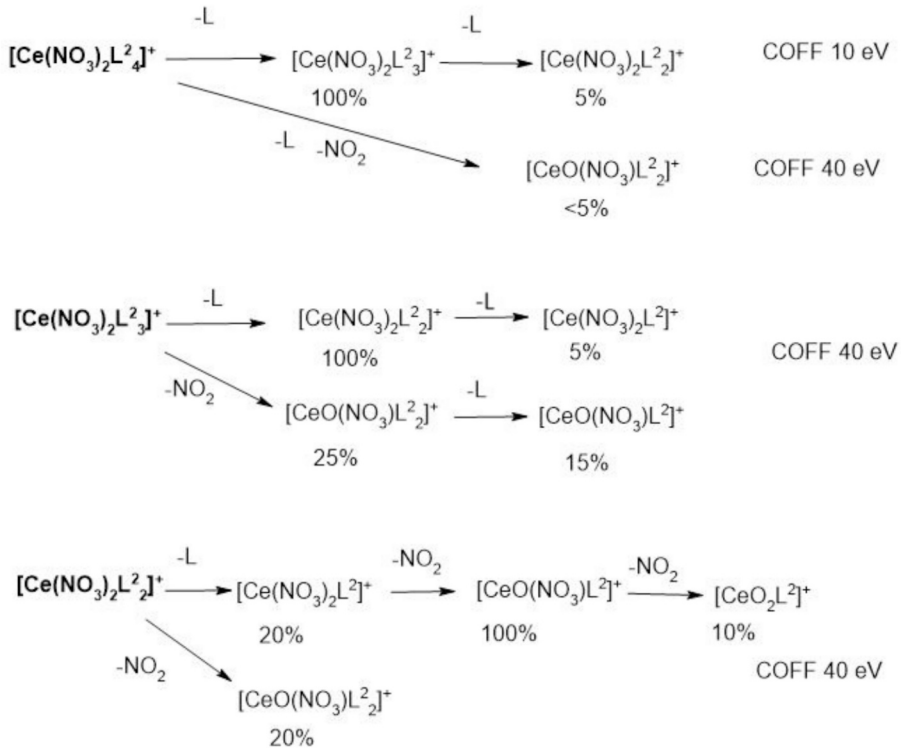

Scheme 2. The main fragmentation pathways for $[Ce(NO_3)_2L^2_n]^+$ ions.

into the formation and stability of Ce(IV) complexes and their stability particularly in the gas phase and in solution.

4. Experimental

4.1. X-ray crystallography

Suitable crystals of each compound were selected, coated in protective perfluoroether oil, and mounted on a MiTeGen holder. Diffraction data were collected on a Rigaku FRE+ diffractometer equipped with VHF Varimax confocal mirrors and a UG2 goniometer and HyPix 6000HE detector or a Rigaku FRE+ equipped with HF Varimax confocal mirrors and an AFC11 goniometer and HG Saturn 724+ detector. The crystals were kept at a steady $T = 100(2)$ K during data collection. The structure was solved with the **ShelXT** [32] structure solution program using the Intrinsic Phasing solution method and by using **Olex2** [33] as the graphical interface. The model was refined with version 2018/3 of **ShelXL** [32]) using Least Squares minimisation. The total number of runs and images was based on the strategy calculation from the program **CrysAlisPro** [34]. All non-hydrogen atoms were refined with anisotropic thermal displacement parameters. Aromatic and aliphatic hydrogen atoms have been included at their geometrically estimated positions. Model refinement was unremarkable, except in the following instances. Further details may, in all cases, be found in the cifs deposited as supplementary information.

Crystallographic data for the structures in this paper have been deposited with the Cambridge Crystallographic Data Centre as supplementary publication numbers CCDC 2500593–2,500,597 for [Ce$(NO_3)_3$(Nap$_2$EtPO)$_3$], [Ce(NO_3)(Nap$_2$MePO)$_3$], [Ce$(NO_3)_4$(Nap$_2$EtPO)$_2$], Nap$_2$EtPO and Nap$_2$MePO respectively. Copies of the data can be obtained, free of charge, on application to CCDC, 12 Union Road, Cambridge CB2 1EZ, UK (Fax: þ44(0)-1223–336,033 or e-mail: deposit@ccdc.cam.ac.uk

4.2. Electrospray ionisation mass spectrometry

Electrospray ionisation mass spectra were recorded on an Agilent iFunnel 6550 Q-TOF LC/MS system. 1 μL of analyte in either chloroform of acetonitrile solution was loop injected in a CH_3CN flow of 0.35 mL / min, nebulisation was assisted by a flow of N_2 at 11 L/min and a source temperature of 130 °C. For tandem mass spectra N_2 at 150 mbar was introduced into the collision chamber. The collision offset voltage was varied from 10 to 40 eV to induce fragmentation of the selected ions.

4.3. NMR spectra

NMR spectra were recorded at 30 °C in $CDCl_3$ or CD_3CN solutions on a JEOL ECX 400 for ^{1}H (399.78 MHz), ^{31}P (161.83 MHz), ^{13}C (100.53 MHz). Approximately 1 mg of solid was dissolved in 1 mL of deuterated solvent.

4.4. Synthesis

Nap$_2$MePO Nap$_3$P (2.65 g, 6.4 mmol) and an excess of MeI (4.23 g, 30 mmol) were heated in a sealed tube on a steam bath for 6 h to give a clear yellow solution. The solution was evaporated to dryness to give Nap$_3$PMe$^+$I$^-$ NMR $CDCl_3$ ^{31}P 22.1 (s),^{13}C 2.1(CH_3)(s), 114.7(CP)(d)$^1J_{PC}$ 86.3 Hz, 125.2(CH)(s), 125.8CH)(d) J_{PC} 15.3 Hz, 128.0(CH)(s), 129.7 (CH)(s), 130.9(CH)(s), 132.1(C)(d) J_{PC} 8.6 Hz, 135.5(C)(d) J_{PC} 9.5 Hz, 137.4(CH)(s), 137.8(CH)(d) J_{PC} 12.5 Hz. The [Nap$_3$MeP]$^+$I$^-$ obtained was stirred under reflux in an ethanol solution of KOH (1.00 g in 15 mL) for 2 h. The ^{31}P NMR showed complete conversion to the phosphine oxide. The mixture was poured into water and the resulting oil stirred overnight with water to give a white powder which was filtered, washed with water, diethyl ether and dried in vacuo over KOH to give 1.66 g (81%). NMR($CDCl_3$) ^{31}P 34.4, ^{13}C 18.3(CH_3)(d)$^1J_{PC}$ 75.5 Hz, 124.7(CH)(d)J_{PC} 14 Hz, 126.5(CH)(s), 126.7(CH)(d) J_{PC} 6 Hz, 127.4(CH)(s), 129.1 (CH)(s), 131.7(CP)(d)$^1J_{PC}$ 99 Hz, 131.6(CH)(d) J_{PC} 11 Hz, 133.3(CH)(d) J_{PC} 2 Hz, 133.3(C)(d) J_{PC} 9 Hz, 134.1(C)(d) J_{PC} 9 Hz.

Nap$_2$EtPO Nap$_3$P (0.73 g 1.8 mmol) was heated in a sealed tube with CH_3CN (3 mL) and an excess of EtI (1.4 g 9.0 mmol) at 80–90 °C for 5 d to give a yellow solution. This was evaporated to dryness to give yellow crystals of Nap$_3$EtP$^+$I$^-$. NMR($CDCl_3$) ^{31}P 30.0, ^{13}C 9.4(CH_3)(d)$^2J_{PC}$ 5 Hz, 20.5 (CH_2)(d)$^1J_{PC}$ 47 Hz, 111.4(C)(d)$^1J_{PC}$ 82 Hz, 125. 0 (CH)(d) J_{PC} 5 Hz, 125.9(CH)(d) J_{PC} 13 Hz, 127.8(CH)(s), 129.6(CH)(s), 130.5(CH)(s), 132.7($C_{4a/8a}$)(d) J_{PC} 8 Hz, 134.3($C_{4a/8a}$)(d) J_{PC} 8 Hz, 137.0(CH) (d) J_{PC} 3 Hz, 137.8(CH)(d) J_{PC} 9 Hz. Nap$_3$EtP$^+$I$^-$ (0.75 g) in 4 ml ethanol was mixed with excess KOH (0.30 g) in 4 ml ethanol and the mixture heated to reflux for 5 h. The yellow solution was evaporated and washed with water and diethyl ether. The solid was recrystallised from chloroform, filtered and evaporated to dryness to give the oxide as a pale yellow solid (0.25 g 42%) NMR($CDCl_3$) ^{31}P 39.2, ^{13}C 6.3(CH_3)(d)$^2J_{PC}$ 4 Hz, 23.6 (CH_2)(d)$^1J_{PC}$ 74 Hz, 129.5(C)(d)$^1J_{PC}$ 92 Hz, 125. 0(CH)(d) J_{PC} 5 Hz, 124.4(CH)(d) J_{PC} 13 Hz, 126.4(CH)(s), 126.7(CH)(d) J_{PC} 5 Hz, 127.3(CH)(s), 129.0(CH) (s), 132.0(CH)(d) J_{PC} 4 Hz, 133.1(CH)(d) J_{PC} 2 Hz 133.6($C_{4a/8a}$)(d) J_{PC} 8 Hz, 134.0($C_{4a/8a}$)(d) J_{PC} 8 Hz.

Crystals of both oxides suitable for x-ray crystallography were prepared by slow diffusion of toluene into a dichoromethane solution of the oxide.

Preparation of] Ce$(NO_3)_3$(Nap$_2$MePO)$_3$] Solutions of Ce$(NO_3)_3$6H$_2$O (0.11 g, 0.25 mmol) in 0.5 g ethanol and Nap$_2$MePO (0.22 g, 0.68 mmol) in 1.6 g ethanol were mixed giving a white precipitate. The mixture was digested on a steam bath for 5 h and the white crystals filtered, washed with erthanol and dried in vacuo to give 0.26 g (90%). Analysis % required (found) C 59.43(60.15) H4.03(4.22) N3.29(3.76).

Preparation of crystals of [Ce$(NO_3)_3$(Nap$_2$MePO)$_3$]. A 5 mm NMR sample tube was charged with Nap$_2$MePO (12.4 mg) and an excess CAN (63.6 mg), (1,3 L^3,CAN), $CDCl_3$ (0.98 g) was added. After 2 weeks the ^{31}P NMR spectroscopy showed a single peak at 51.2 ppm. The solution was allowed to slowly evaporate and the small quantity of crystals formed collected for x-ray diffraction.

Preparation of crystals of [Ce$(NO_3)_4$(Nap$_2$EtPO)$_2$CDCl$_3$] . A 5 mm NMR sample tube was charged with Nap$_2$EtPO (4.4 mg) and an excess CAN (26.1 mg), (1,3.6 L,CAN) $CDCl_3$ (1.07 g) was added and the reaction monitored by ^{31}P NMR spectroscopy for 2 weeks by which time the spectrum showed a single peak at 54.9 ppm. The solution was separated from undissolved solid and transferred to a separate 5 mm NMR tube and the solution slowly evaporated. Small brown / red crystals formed at the solvent air interface and were separated. Analysis % required (found) C 46.23(45.82) H3.45(3.29) N4.79(5.74).

Preparation of crystals of [Ce$(NO_3)_3$(Nap$_2$EtPO)$_3$]. A 5 mm NMR sample tube was charged with Nap$_2$EtPO (9.8 mg) and an excess CAN (35.6 mg), (1,2 L^3:CAN), CD_3CN (0.55 g) was added and the reaction monitored by ^{31}P NMR spectroscopy the spectrum initially showed a single peak at 54.9 ppm. The crystals that formed during slow evaporation were separated and collected for x-ray diffraction. There was insufficient material for elemental analysis.

Declaration of competing interest

The authors declare that they have no known competing financial interests or personal relationships that could have appeared to influence the work reported in this paper.

Acknowledgements

We are grateful to the EPSRC for the use of the National Crystallography Service at Southampton University [35].

There are no conflicts of interest associated with the paper or any of the authors.

Appendix A. Supplementary data

Supplementary data to this article can be found online at https://doi.org/10.1016/j.ica.2026.123180.

Data availability

Data will be made available on request.

References

[1] S.A. Cotton, Lanthanide and Actinide Chemistry, John Wiley & Sons, Chichester, England, 2006.
[2] H. Tsurugi, K. Mashima, J. Am. Chem. Soc. 143 (2021) 7879–7890.
[3] H.-L. Phan, X. Jiang, Q. Yan, Y.-M. So, W. Chan, H.H.Y. Sung, I.D. Williams, Inorg. Chem. 63 (2025) 1433–1442.
[4] J. Lv, Y. Lang, C.J. Li, H. Zeng, Chem. Commun. 61 (2025) 4054–4057.
[5] Y.-C. Lu, H.M. Jordan, J.G. West, Chem. Commun. 57 (2021) 1871–1874.
[6] Y. Lee, H. Ki, D. Im, S. Eom, J. Gu, S. Lee, J. Kim, Y. Cha, K.W. Lee, S. Zerdane, M. Levantino, H. Ihee, J. Am. Chem. Soc. 145 (43) (2023) 23715–23726.
[7] J. Jacobsen, A. Ienco, R. D'Amato, F. Constantino, N.D. Stock, Dalton Trans. 49 (2020) 16551–16586.
[8] J.X. Gu, H. Chen, Y. Ren, Z.-G. Gu, G. Li, W.-J. Xu, X.-Y. Yang, J.-X. Wen, J.-T. Wu, H.-G. Jin, Chemsuschem 15 (2022) e202102368.
[9] S. Kandambeth, R. Kancherla, K. Pal, T. Melliti, M. Zeama, V.S. Kale, I. Nadinov, A. M. Alali, O. Shekhah, O.F. Mohammed, M. Rueping, M. Eddaoudi, Angew. Chem. Int. Ed. 64 (2025) e202503328.
[10] Z. Yang, S. Xu, H. Du, J. Li, T. Peng, C. Liu, Angew. Chem. Int. Ed. 64 (2025) e202508960.
[11] A. Aliabadi, S. Abdolmaleki, S. Khaksar, J. Mol. Struct. 1319 (2025) 139377.
[12] Y.-M. So, W.-H. Leung, Coord. Chem. Rev. 340 (2017) 172–197.
[13] A.W.G. Platt, Coord. Chem. Rev. 340 (2017) 62–78.
[14] M. Ul-Haque, C.N. Caughlin, F.A. Hart, R. van Nice, Inorg. Chem. 10 (1971) 115–122.
[15] J. Lin, E. Hey-Hawkins, H.G. von Schnering, Z. Naturforsch. 45a (1990) 1241–1247.
[16] S.J. Coles, S.J. Fieldhouse, W.T. Klooster, A.W.G. Platt, Polyhedron 161 (2019) 346–351.
[17] S.J. Coles, S. Cooper, W.T. Klooster, L.J. McCormick Mc Pherson, A.W.G. Platt, Eur. J. Inorg. Chem. 26 (2023) e202300375.
[18] S.J. Coles, S. Cooper, W.T. Klooster, L.J. McCormick Mc Pherson, A.W.G. Platt, K. Singh, Molecules 29 (2024) 2580.
[19] J.W. Emsley, S.R. Salaman, R.A. Storey, J. Chem Soc. B (1970) 1513–1516.
[20] V. Butera, L. D'Anna, S. Rubino, R. Bonsignore, A. Spinello, A. Terenzi, G. Barone, J. Phys. Chem. A 127 (2023) 9283–9290.
[21] L. Pazderski, T. Pawlak, J. Sitkowski, L. Kozerski, E. Szlyk, Magn. Reson. Chem. 48 (2010) 417–426.
[22] S. Alvarez, P. Alemany, D. Casanova, J. Cirera, M. Llunell, Avnir, D Coord. Chem. Rev. 249 (2005) 1693–1708.
[23] M. Llunell, D. Casanova, J. Cirera, P. Alemany, S. Alvarez, SHAPE—Program for the Stereochemical Analysis of Molecular Fragments by Means of Continuous Shape Measures and Associated Tools, Version 2.1, University of Barcelona, Spain, 2013. Shape.
[24] E. Pilichos, A. Tubau, S. Speed, M. Font-Buria, A. Escuer, A. Grabulosa, J. Mayans, Dalton Trans. 52 (2023) 2485–2494.
[25] J. Lin, E. Hey, H.G. von Schnering, CSD Comm. (1994).
[26] W. Levason, E.H. Newman, W. Webster, Acta Cryst C 56 (2000) 1308–1309.
[27] L. Massai, C. Zoppi, D. Cirri, A. Pratesi, L. Messori, Front. Chem. 8 (2020) 581648.
[28] C. Heinemann, H.H.Cornehl, D.Schröder, M.Dolg, H. Schwartz, Inorg. Chem. 35 (9) (1996) 2463–2475.
[29] Q. Zhang, S.-X. Hu, H. Qu, J. Su, G. Wang, J.-B. Lu, M. Chen, M. Zhou, J. Li, Angew. Chem. Int. Ed. (2016) 6896–6900.
[30] T.Madanhive, L-C.C.Coetzee, T.J.Rashamuse, N.P.Magwa, Inorg. Chem. Comm. 176 (2025) 114218.
[31] M.J.Y. Jarvis, V. Blagojevic, G.K. Koyanagi, D.K. Bohme, Phys. Chem. Chem. Phys. 12 (2010) 4852–4862.
[32] G.M. Sheldrick, C27, 3–8; Sheldrick, G.M., ShelXT-Integrated space-group and crystal-structure determination, Acta Cryst. **A71** (2015) 3–8.
[33] O.V. Dolomanov, L.J. Bourhis, R.J. Gildea, J.A.K. Howard, H. Puschmann, Olex2: a complete structure solution, refinement and analysis program, J. Appl. Cryst. 42 (2009) 339–341.
[34] Rigaku Oxford Diffraction (Ed.), CrysAlisPro Software System, 2019.
[35] S.J. Coles, P.A. Gale, Chem. Sci. 3 (2012) 68.